

Making other earths: dynamical simulations of terrestrial planet formation and water delivery

Sean N. Raymond,^{a,*} Thomas Quinn,^a and Jonathan I. Lunine^b

^a Department of Astronomy, University of Washington, Box 351580, Seattle, WA 98195, USA

^b Lunar and Planetary Laboratory, The University of Arizona, Tucson, AZ 85287, USA

Received 6 August 2003; revised 12 November 2003

Abstract

We present results from 44 simulations of late stage planetary accretion, focusing on the delivery of volatiles (primarily water) to the terrestrial planets. Our simulations include both planetary “embryos” (defined as Moon to Mars sized protoplanets) and planetesimals, assuming that the embryos formed via oligarchic growth. We investigate volatile delivery as a function of Jupiter’s mass, position and eccentricity, the position of the snow line, and the density (in solids) of the solar nebula. In all simulations, we form 1–4 terrestrial planets inside 2 AU, which vary in mass and volatile content. In 44 simulations we have formed 43 planets between 0.8 and 1.5 AU, including 11 “habitable” planets between 0.9 and 1.1 AU. These planets range from dry worlds to “water worlds” with 100+ oceans of water (1 ocean = 1.5×10^{24} g), and vary in mass between $0.23M_{\oplus}$ and $3.85M_{\oplus}$. There is a good deal of stochastic noise in these simulations, but the most important parameter is the planetesimal mass we choose, which reflects the surface density in solids past the snow line. A high density in this region results in the formation of a smaller number of terrestrial planets with larger masses and higher water content, as compared with planets which form in systems with lower densities. We find that an eccentric Jupiter produces drier terrestrial planets with higher eccentricities than a circular one. In cases with Jupiter at 7 AU, we form what we call “super embryos,” $1-2M_{\oplus}$ protoplanets which can serve as the accretion seeds for $2 + M_{\oplus}$ planets with large water contents.

© 2003 Elsevier Inc. All rights reserved.

Keywords: Planetary formation; Extrasolar planets; Origin, Solar System; Cosmochemistry; Exobiology

1. Introduction

There is a paradox in the definition of the habitable zone with respect to the presence of liquid water. Imagine a planet at the right distance from a star to have stable liquid water on its surface, supported by a modest greenhouse effect. Nebular models and meteorite data suggest that the local environment during the early formation of this planet was sufficiently hot to prevent hydration of the planetesimals and protoplanets out of which the planet was formed (Morbidelli et al., 2000). That is, the local building blocks of this “habitable” planet were devoid of water. How, then, could this planet acquire water and become truly habitable? Delivery of water-laden planetesimals from colder regions of the disk is one solution, but it implies that the habitability of extrasolar planets depends on the details of their final assembly, with

implications for the abundance of habitable planets available for Terrestrial Planet Finder (TPF) to discover.

In the current paradigm of planet formation four dynamically distinct stages are envisioned (Lissauer, 1993):

Initial stage: Grains condense and grow in the hot nebular disk, gradual settling to the mid-plane. The composition of the grains is determined by the local temperature of the nebula. Gravitational instability among the grains is resisted owing to continuous stirring by convective and turbulent motions.

Early stage: Growth of grains to km-sized planetesimals occurs via pairwise accretion in the turbulent disk, or possibly via gravitational instability under certain nebular conditions (Goldreich and Ward, 1973; Youdin and Shu, 2002). Planetesimals initially have low eccentricities (e) and inclinations (i) due to gas drag.

Middle stage—oligarchic growth: “Focused merging”—accretion with gravitationally augmented cross

* Corresponding author.

E-mail address: raymond@astro.washington.edu (S.N. Raymond).

sections—leads to agglomeration of planetesimals into Moon-to Mars-sized “planetary embryos.” Possible runaway accretion and subsequent energy equipartition (dynamical friction) may lead to polarization of the mass distribution: a few large bodies with low e and i in a swarm of much smaller planetesimals with high e and i . The timescale for this process correlates inversely with heliocentric distance. Simulations of oligarchic growth by Kokubo and Ida (2000) suggest that planetary embryos form in < 1 Myr at 1 AU, in ~ 40 Myr at 5 AU, and in > 300 Myr past 10 AU. Since the giant planets are constrained to have formed within 10 Myr from inferred lifetimes of gaseous disks around young stars (Briceño et al., 2001), embryos could only have formed in the innermost Solar System within that time. Thus, we expect that at the time of the formation of Jupiter, the inner terrestrial region was dominated by ~ 30 – 50 planetary embryos while the asteroid belt consisted of a large number of ~ 1 km planetesimals.

Note that this scenario is based on a relatively low surface density model, and is somewhat inconsistent with the “core accretion” model for the formation of giant planets (Pollack et al., 1996), which requires solid accretion cores of several Earth masses to form between 5 and 10 AU in less than 10 Myr, presumably by oligarchic growth. The formation timescale and masses of planetary embryos are sensitive to the surface density (Kokubo and Ida, 2002), and the detailed mass distribution in the disk at the time of Jupiter’s formation is unclear.

Late Stage: Once runaway accretion has terminated due to lack of slow moving material, planetary embryos and planetesimals gradually evolve into crossing orbits as a result of cumulative gravitational perturbations. This leads to radial mixing and giant impacts until only a few survivors remain. The timescale for this process is $\sim 10^8$ yr.

Until recently, a leading hypothesis for the origin of Earth’s water was the “late veneer” scenario, in which the Earth formed primarily from local material, and acquired its water at later times from a large number of cometary impacts. These impacts resulted in a hot water vapor atmosphere which condensed into oceans (Matsui and Abe, 1986). However, the D/H ratio of three comets has been measured to be 12 times higher than the protosolar value (Balsiger et al., 1995; Meier et al., 1998; Bockelee-Morvan et al., 1998), and roughly twice the terrestrial oceanic (roughly the chondritic) value. This implies that at most 10% of the Earth’s water came from a cometary source (Morbidelli et al., 2000).

Morbidelli et al. (2000) proposed that the bulk of the Earth’s water may have come from the asteroid belt in the form of planetary embryos. The proto-Earth accreted several

embryos from outside its local region, including a few from past 2.5 AU, which delivered the bulk of the Earth’s water. In this model the Earth accreted water since its formation, in the form of an early bombardment of asteroids and comets, a few large “wet” planetary embryos, and continual impacts of small bodies over long timescales. This scenario explains the D/H ratio of Earth’s water in the context of late-stage planetary accretion.

Morbidelli et al. (2000) assumed that oligarchic growth took place throughout the inner Solar System, with planetary embryos out to 4 AU. If the timescale for the formation of Jupiter is less than that for planetary embryos in the outer asteroid belt (past 2.5 AU), these initial conditions neglect Jupiter’s strong gravitational influence on the oligarchic growth process in the asteroid belt, as well as planetesimal–embryo interactions. Several other authors (e.g., Chambers, 2001; Chambers and Cassen, 2002) subsequently have numerically formed terrestrial planets, including both planetary embryos and planetesimals in their simulations. Their initial conditions often seem ad hoc, and not based on the state of the protoplanetary disk at the end of oligarchic growth, in particular the radial dependence of the planetary embryo formation timescale, which depends in turn on the surface density of the disk (Kokubo and Ida, 2002).

Chambers (2003) used a statistical Öpik–Arnold method to test planet formation in a number of scenarios, including some which are similar to those we present in this paper. The advantage of his statistical method is its low computational expense relative to N -body simulations, allowing the quick exploration of a large parameter space. Its drawback is the difficulty of implementing realistic dynamics. Therefore, N -body simulations like those we present here may be used to “calibrate,” and thereby complement the statistical simulations.

In this paper, we characterize the process of terrestrial planet formation and volatile delivery as a function of several parameters of the protoplanetary system. Our initial conditions attempt to realistically describe the protoplanetary disk at the beginning of late-stage accretion, assuming a relatively low density protoplanetary disk in which oligarchic growth proceeds as described above. We do not limit ourselves to our own Solar System, and focus on the formation of planets within the habitable zone of their parent stars. The parameters we vary in our simulations are

- (i) Jupiter’s mass,
- (ii) eccentricity,
- (iii) semimajor axis, and
- (iv) time of formation,
- (v) the density in solids of the protoplanetary disk, and
- (vi) the location of the snow line.

Section 2 describes our initial conditions and numerical methods. Section 3 presents our results, which are discussed in Section 4, including application to the NASA’s Terrestrial Planet Finder (TPF) mission. Section 5 concludes the paper.

2. Model

2.1. Initial conditions

The timescale for the formation of planetary embryos from planetesimals correlates with heliocentric distance (Kokubo and Ida, 2000). We wish to accurately describe the state of the protoplanetary disk at the time when Jupiter formed. (Note that we use the term ‘‘Jupiter’’ to represent the gas giant planet in each planetary system, the majority of which differ from our Solar System.) We assume that oligarchic growth has taken place in the inner Solar System, from 0.5 AU to the 3 : 1 mean motion resonance with Jupiter, located at 2.5 AU in our Solar System. The timescale for embryos to form out to 2.5 AU is roughly 10 Myr, assuming a surface density 50% more massive than the minimum-mass nebula model (Kokubo and Ida, 2000, and references therein). 10 Myr is also the upper bound for the time of Jupiter’s formation (Briceño et al., 2001). Past the 3 : 1 resonance, we expect the gravitational influence of Jupiter to perturb the oligarchic growth process, through the clearing out of resonances and other dynamical excitation of planetesimals.

Between the 3 : 1 resonance and Jupiter we assume that the mass in solids is in the form of planetesimals. Since we are computationally limited to a small number of particles (~ 200) we cannot accurately represent the billions of planetesimals in this region. We treat this problem in two ways:

- (i) All the mass in the asteroid belt is divided into N ‘‘super-planetesimals’’ with $M_{\text{planetesimal}} = M_{\text{ast}}/N$, where M_{ast} is the total mass in the region.
- (ii) The planetesimal mass is fixed at 0.01 Earth masses (M_{\oplus}).

In both cases the number of planetesimals is ~ 150 , and they are distributed as $N \propto r^{-1/2}$, corresponding to the annular mass in a disk with surface density $\Sigma \propto r^{-3/2}$. In case (i), the entire mass in the region (M_{ast}) is accounted for, but the ‘‘planetesimals’’ have masses $\sim 0.1M_{\oplus}$ ($\simeq M_{\text{Mars}}$). In case (ii), the planetesimal masses are somewhat more realistic, but we do not account for the entire mass inventory in the region. Case (i) will provide a rough upper limit on the mass in volatiles delivered to the terrestrial planets, while case (ii) corresponds to a lower limit. Case (ii) only accounts for $\sim 10\%$ of the mass in the asteroid region, as predicted by Eq. (1). Therefore, these simulations are also a test of the effects of the surface density past the snow line on the forming terrestrial planets and their composition.

In neither of these cases are the planetesimals truly that, as their masses are comparable to those of planetary embryos. Their large masses and small number nullify the effects of dynamical friction, a likely mechanism for damping the eccentricities of protoplanets. However, as discussed above, we do not expect fully grown planetary embryos to have formed in the outer asteroid belt at this time, and we

therefore effectively begin our simulations in the late stages of oligarchic growth with many smaller planetary embryos, neglecting the eccentricity damping of true, ~ 1 km planetesimals. In this way we attempt to take Jupiter’s presence into account during oligarchic growth in the outer asteroid region.

We use a two-tiered surface density profile similar to Kokubo and Ida (2000), which reflects an increase in surface density due to the condensation of water immediately past the snow line:

$$\Sigma(r) = \begin{cases} \Sigma_1 r^{-3/2}, & r < \text{snow line}, \\ \Sigma_{\text{snow}} \left(\frac{r}{5\text{AU}}\right)^{-3/2}, & r > \text{snow line}. \end{cases} \quad (1)$$

The ‘‘feeding zone’’ of a planetary embryo is an annulus with width comparable to the embryo’s Hill radius,

$$R_{\text{H}} = a \left(\frac{M}{3M_{\odot}} \right)^{1/3}, \quad (2)$$

where a is the embryo’s semimajor axis, M is its mass, and M_{\odot} is the solar mass. The mass in the feeding zone of an embryo is

$$M = 2\pi a \Sigma R_{\text{H}}. \quad (3)$$

Assuming that the mass of an embryo is proportional to the mass in the feeding zone, it follows from the surface density profile in Eq. (1) that the mass of a planetary embryo $M_{\text{embryo}} \propto a^{3/4}$. Simulations of the formation of embryos from planetesimals (Kokubo and Ida, 2000) show that they typically form with separations of 5–10 mutual Hill radii, rather than immediately adjacent to each other in heliocentric distance, where the mutual Hill radius of bodies 1 and 2 is defined as

$$R_{\text{H},m} = \left(\frac{a_1 + a_2}{2} \right) \left(\frac{M_1 + M_2}{3M_{\odot}} \right)^{1/3}. \quad (4)$$

We therefore space the planetary embryos inside the 3 : 1 resonance by Δ mutual Hill radii (i.e., $a_{n+1} = a_n + \Delta R_{\text{H},m}$), with Δ varying randomly between 5 and 10. So the mass of an embryo increases as

$$M_{\text{embryo}} \propto a^{3/4} \Delta^{3/2} \Sigma_1^{3/2}. \quad (5)$$

A snow line at 2.5 AU corresponds, by coincidence, to the location of the 3 : 1 resonance for a Jupiter at 5.2 AU. This implies that, in our Solar System, the local surface density increase at the snow line implied by Eq. (1) is not reflected in the masses of planetary embryos, as they only form interior to the snow line. If Jupiter’s semimajor axis is less than 5.2 AU the situation is the same, as the 3 : 1 resonance is located interior to the snow line. However, if Jupiter’s orbit is larger than 5.2 AU, then the 3 : 1 resonance is exterior to the snow line, and there is a region in which oligarchic growth has taken place in a high density environment. As a consequence of Eq. (5), this results in the formation of what we call ‘‘super embryos,’’ which can have masses as large as $2M_{\oplus}$. These large icy bodies probably did not form in our

Solar System, but their dynamical presence can affect terrestrial planet formation interior to their orbits (see Section 3).

In our simulations, we vary the following parameters:

- (1) The semimajor axis of Jupiter’s orbit: $a_J = 4, 5.2$ or 7 AU. Levison et al., 1998 showed that a wide variety of systems of giant planets can exist. In this treatment, we restrict ourselves to the case of a single giant planet in order to clearly evaluate the significance of different parameters on the terrestrial planets which form in these systems.
- (2) Jupiter’s mass: $M_J = 10M_\oplus, \frac{1}{3}M_{J,r}, M_{J,r}$ or $3M_{J,r}$, where $M_{J,r}$ is Jupiter’s real mass of 318 Earth masses.
- (3) The eccentricity of Jupiter’s orbit: $e_J = 0, 0.1$, or 0.2 .
- (4) The location of the snow line: 2, 2.5 or 5 AU. A snow line at 2 AU results in the formation of “super embryos” for Jupiter at 5.2 AU. There is no break in the surface density profile, as prescribed by Eq. (1), for a snow line at 5 AU. See Section 2.2 for a discussion of these values.
- (5) The surface density of solids: $\Sigma_1 = 8\text{--}10 \text{ g cm}^{-2}$, $\Sigma_{\text{snow}} = 3\text{--}4 \text{ g cm}^{-2}$. Note that the minimum mass solar nebula has $\Sigma_1 = 6 \text{ g cm}^{-2}$.
- (6) The planetesimal mass (exterior to the 3 : 1 resonance): case (i) $M_{\text{planetesimal}} = M_{\text{ast}}/N_{\text{planetesimal}}$ or case (ii) $M_{\text{planetesimal}} = 0.01M_\oplus$, where $N_{\text{planetesimal}} = 150$. We emphasize that these masses are comparable to those of planetary embryos, and that the distinction between what we call “planetesimals” and “planetary embryos” has to do with the location and timescale of their formation, as described above.
- (7) The time of Jupiter formation: Jupiter forms at $t = 0$, or starts as a $10M_\oplus$ seed whose mass increases to M_J at $t = 10$ Myr. Note that in three simulations Jupiter’s mass was not increased to M_J , but left at $10M_\oplus$. 10 Myr was chosen as an upper limit to the timescale of giant planet formation (Briceño et al., 2001).

Figure 1 shows the initial distribution of planetary embryos and planetesimals for two simulations, showing the range in variation of these parameters. Table 1 lists the initial conditions for all 44 simulations.

2.2. Water content

The water content of planetesimals in a given planetary system depends in a complex way upon a range of factors including the mass and evolutionary characteristics of the protoplanetary disk, overall metallicity of the molecular cloud clump from which the star is forming, and the positions, masses and timings of formation of the system’s giant planets. Although in this paper we track the dynamical history of planetesimals for a given set of giant planet orbital parameters, our model is not capable of determining the water content of the planetesimals versus semimajor axis, in part because this is determined long before the stage at which planetesimals grow to the size of the Moon or larger. How-

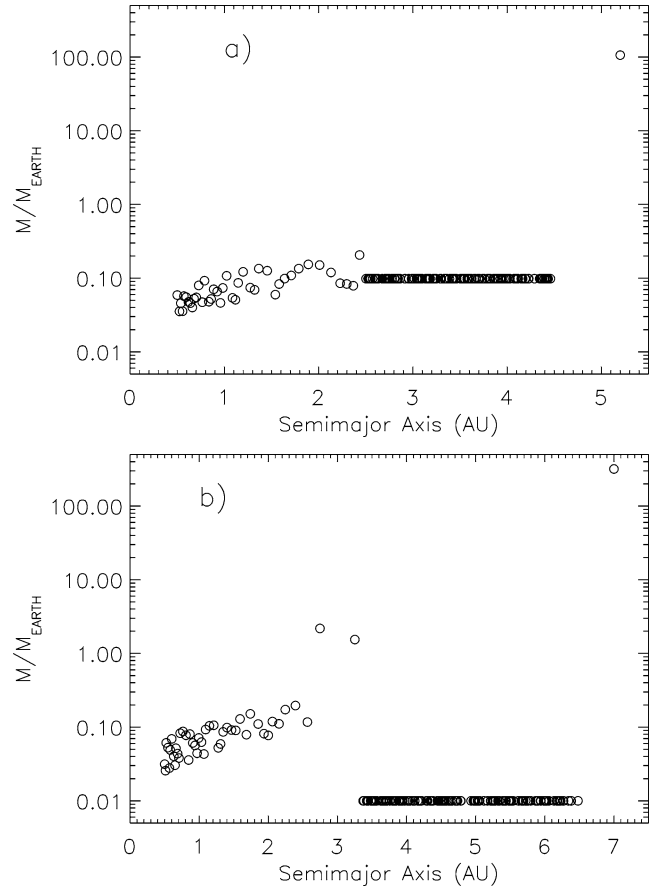


Fig. 1. Initial conditions for two simulations. In the simulation from panel (a), Jupiter’s semimajor axis is 5.2 AU and its mass is 1/3 of its real mass. Planetary embryos are present inside the 3 : 1 resonance at 2.5 AU, and their masses are increasing with semimajor axis. As the separation of embryos Δ varies randomly between 5 and 10 mutual Hill radii, the embryos mass fluctuates according to Eq. (5). In panel (a) the planetesimal mass is $\sim 0.1M_\oplus$, and all of the mass in the asteroid belt is contained in these 150 planetesimals. In the simulation from panel (b), Jupiter’s semimajor axis is 7 AU, and its mass is equal to its current mass. In this case the 3 : 1 resonance lies outside the snow line, so there is a region between 2.5 and 3.36 AU in which $1\text{--}2M_\oplus$ “super embryos” have formed. The planetesimal mass in this simulation is $0.01M_\oplus$. Table 1 summarizes the initial conditions for all 44 simulations.

ever, it should be said that even nebular models concerned with earlier stages of planetesimal growth lack the fidelity to create ab initio a reliable map of water content versus semimajor axis. In this paper we assume a distribution of water content versus semimajor axis for the planetesimals, in all of our model systems, based on the meteorite data for our own Solar System. The stochastic delivery of water to the terrestrial planets that is one of the main conclusions of this paper argues against any more detailed attempt to scale the water abundance for any given system according to disk parameters, for the resulting delivery of water will remain stochastic.

Figure 2 gives the range of water content, by mass, of three types of chondritic meteorites compared to an estimate for the Earth. Carbonaceous chondrites are the most

Table 1
Initial conditions for 44 simulations

Simulation	a_J (AU)	e_J	M_J ($M_{J,r}$) ^a	t_J (Myr) ^b	M_{pl} (M_{\oplus}) ^c	Σ_1 (g cm^{-2})	Σ_{snow} (g cm^{-2})	Snow line (AU)
1	4.0	0.0	1	0	0.09	10	4	2.5
2	4.0	0.0	1	0	0.09	10	4	2.5
3	4.0	0.0	1	0	0.09	10	4	2.5
4	5.2	0.0	1	0	0.09	10	4	2.5
5	5.2	0.0	1	0	0.09	10	4	2.5
6	5.2	0.0	1	0	0.09	10	4	2.5
7	7.0	0.0	1	0	0.11	10	4	2.5
8	7.0	0.0	1	0	0.11	10	4	2.5
9	7.0	0.0	1	0	0.11	10	4	2.5
10	5.2	0.0	1	0	0.01	10	3	2.5
11	5.2	0.0	1	0	0.01	10	3	2.5
12	5.2	0.0	1	0	0.01	8	3	2.5
13	5.2	0.0	1	0	0.01	8	3	2.5
14	7.0	0.0	1	0	0.01	8	3	2.5
15	7.0	0.0	1	0	0.01	8	3	2.5
16	4.0	0.0	1	0	0.01	8	3	2.5
17	4.0	0.0	1	0	0.01	8	3	2.5
18	5.2	0.0	1	0	0.01	8	3	2.0
19	5.2	0.0	1	0	0.01	8	3	2.0
20	7.0	0.0	1	0	0.01	8	3	2.0
21	7.0	0.0	1	0	0.01	8	3	2.0
22	5.2	0.0	1/3	0	0.01	10	4	2.5
23	5.2	0.0	1/3	0	0.01	10	4	2.5
24	5.2	0.0	1/3	0	0.10	10	4	2.5
25	5.2	0.0	1/3	0	0.10	10	4	2.5
26	5.2	0.0	3	0	0.01	10	4	2.5
27	5.2	0.0	3	0	0.01	10	4	2.5
28	5.2	0.0	3	0	0.10	10	4	2.5
29	5.2	0.0	3	0	0.10	10	4	2.5
30	5.2	0.1	1	0	0.01	10	4	2.5
31	5.2	0.1	1	0	0.01	10	4	2.5
32	5.2	0.1	1	0	0.01	10	4	2.5
33	5.2	0.2	1	0	0.01	10	4	2.5
34	5.2	0.2	1	0	0.01	10	4	2.5
35	5.2	0.2	1	0	0.01	10	4	2.5
36	5.5	0.0	1	10	0.01	10	4	2.5
37	5.5	0.0	1	10	0.01	10	4	2.5
38	5.5	0.0	1	10	0.01	10	4	2.5
39	5.5	0.0	1	10	0.01	10	4	2.5
40	5.5	0.0	0.03	0	0.01	10	4	2.5
41	5.5	0.0	0.03	0	0.01	10	4	2.5
42	5.5	0.0	0.03	0	0.01	10	4	2.5
43	5.5	0.0	1	0	0.05	10	4	5
44	5.5	0.0	1	0	0.05	10	4	5

^a Jupiter's mass, in units of its real mass $M_{J,r}$. In simulations 40–42, Jupiter's mass is $10M_{\oplus}$.

^b Time of Jupiter formation. For simulations with $t_J = 10$ Myr, Jupiter began the simulation as a $10M_{\oplus}$ accretion seed and was inflated to Jupiter's real mass at 10 Myr.

^c The mass of a planetesimal, in Earth masses. Referred to as $m_{\text{planetesimal}}$ in text.

water rich of meteorites, with water content up to nearly 10% by mass. The ordinary chondrites are significantly lower, roughly by an order of magnitude, and the enstatite chondrites are somewhat lower still (Abe et al., 2000). The locations within our Solar System from which the parent bodies of the meteorites were derived is highly uncertain, though it is generally thought that the carbonaceous chondrites came from the region beyond 2.5 AU, while the ordinary and enstatite chondrites were formed further inward. Earth, for which no primitive counterpart exists in the meteorite record discovered to date (Drake and Righter, 2002), is quite dry

with a water content around 0.03–0.1% by mass (Abe et al., 2000). Much of this may have been added from planetesimals at larger semimajor axes than 1 AU (Morbidelli et al., 2000), consistent with the dynamical results we present below. Also, the lunar-forming impactor appears to have been extremely dry, with water content much less than that of the Earth (Abe et al., 2000). Hence, planetesimals at 1 AU could have been orders of magnitude dryer than the water content of the Earth today.

Hydration of the silicates in meteorites is thought to have occurred inside a parent body rather than in the solar nebula,

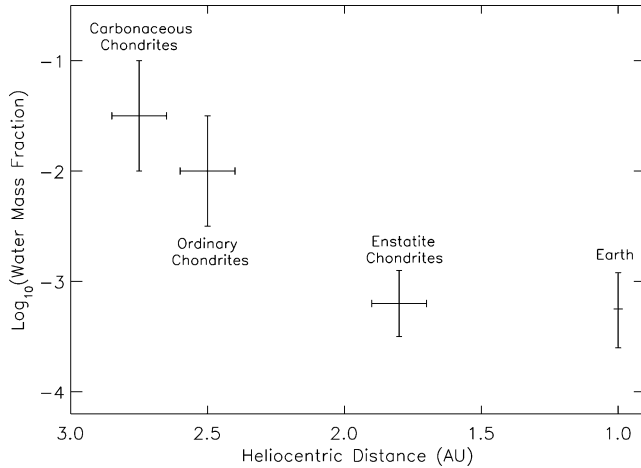


Fig. 2. Water content of various types of chondrites in our Solar System, with approximate values for the positions of the parent bodies. Water percentages from Abe et al. (2000).

due to the very long hydration timescales in the solar nebula (Fegley, 2000). This implies that hydrated bodies could only form by accreting ice, which then reacted as liquid water with the anhydrous minerals when sufficiently heated (by radioactive, frictional or collisional heating). The current distribution of water-rich vs. dry classes of asteroids may be a record of the position of the snow line in the solar nebula (neglecting possible orbital migration of asteroids). This division occurs at roughly 2–2.5 AU in our Solar System, and corresponds to a nebular temperature of ~ 170 K (Hayashi, 1981). A density increase immediately past the snow line is expected due to the “cold trap” effect (Stevenson and Lunine, 1988), and is expressed in Eq. (1).

There is a large uncertainty in the position of the snow line in the solar nebula. The standard notion of a snow line around 4–5 AU can explain the rapid formation of Jupiter in a high density environment immediately past the snow line. However, as mentioned above, volatile-rich classes of asteroids are found as close as 2–2.5 AU, and are presumably a fossil record of ice-bearing material. Models of protoplanetary disks around T Tauri stars by Sasselov and Lecar (2000) result in snow lines as close as 1 AU to the central stars, depending primarily on the stellar luminosity and the rate of accretional heating within the disk. As these quantities evolve with time, so might the position of the snow line migrate change with time. The nebular models of Bell et al. (1997) show that the temperature profile of the disk changes with the mass accretion rate therein, which should decrease monotonically with time. The position in the nebula at 170 K moves inward in time, from past 10 AU for $\dot{M} = 10^{-5} M_{\odot} \text{ yr}^{-1}$ to inside 1 AU for $\dot{M} = 10^{-9} M_{\odot} \text{ yr}^{-1}$ (Fig. 1 from Bell et al., 1997). If one assumes a constant total rate of mass accretion as a function of time of $0.1 M_{\odot} \text{ yr}^{-1}$, the time spent by the nebula in various stages of evolution can be inferred (Monika Kress, personal communication). The 170 K radius moves approximately from 4–5 AU at

1 Myr to 1.5–3 AU at 10 Myr (inferred from Fig. 1 of Bell et al., 1997, and Fig. 3 of Bell et al., 2000).

We expect planetary embryos to form anywhere the timescale for their formation is shorter than the timescale for disruption. The formation timescale depends strongly on the local surface density, which is enhanced past the snow line by the condensation of water vapor into ice. Disruption occurs in the central Solar System via the formation of Jupiter and Saturn, whose gravitational influence plays a large part in the dynamics of planetesimals from 2.5 to 20 AU. This scenario is further complicated by the inward drift of the snow line, causing the formation timescale of embryos to vary with time. In certain regions “super embryos” may form, perhaps at very early times in the Jupiter–Saturn region. It is also conceivable that in certain circumstances these super-embryos may form further in, on a timescale comparable to that for the dissipation of gas from the disk. We form such systems when the 3 : 1 Jupiter resonance lies exterior to the snow line (see Section 2.1).

Our choice of a snow line at 2.5 AU is close to that for the “minimum-mass solar nebula” model of Hayashi (1981), and lies in a range consistent with the asteroid data. We have also run a small number of simulations with snow lines at 2 and 5 AU, to test the sensitivity our model to its location. These are discussed in the Results section.

As a baseline, we divide each of the planetary systems into three regions according to water content—planetesimals beyond 2.5 AU have 5% water by mass, those inward of 2 AU have water content of 0.001% by mass, and between 2–2.5 AU lie planetesimals with intermediate water content of 0.1% by mass. This distribution of water among the planetesimals can be seen in the first panel of the accretion simulations we show below (Fig. 3, for example). The results of our calculations are such that the intermediate planetesimal class, in terms of water content, does not affect the overall conclusions regarding delivery of water to Earth. Thus, one can think of the simulations as positing two regions—one water-rich beyond 2–2.5 AU and one water poor inward of that—and then following through the collisional history of the planetesimals the delivery of water to the final few terrestrial planets remaining at the end of each simulation.

2.3. Numerical method

We integrate all simulations for 200 Myr using Mercury (Chambers, 1999). We use the hybrid integrator, which uses a second-order mixed variable symplectic algorithm when objects are separated by more than 3 Hill radii, and a Burlisch–Stoer method for closer encounters. Planetary embryos and “planetesimals” are both self-gravitating, and treated in the same way. We use a 6 day timestep, in order to have 15 timesteps per orbit for the innermost orbits in our initial conditions at 0.5 AU. Our simulations conserve energy to better than 1 part in 10^4 , and angular momentum to 1 part in 10^{11} . Collisions conserve linear momentum and do not take fragmentation into account. These simula-

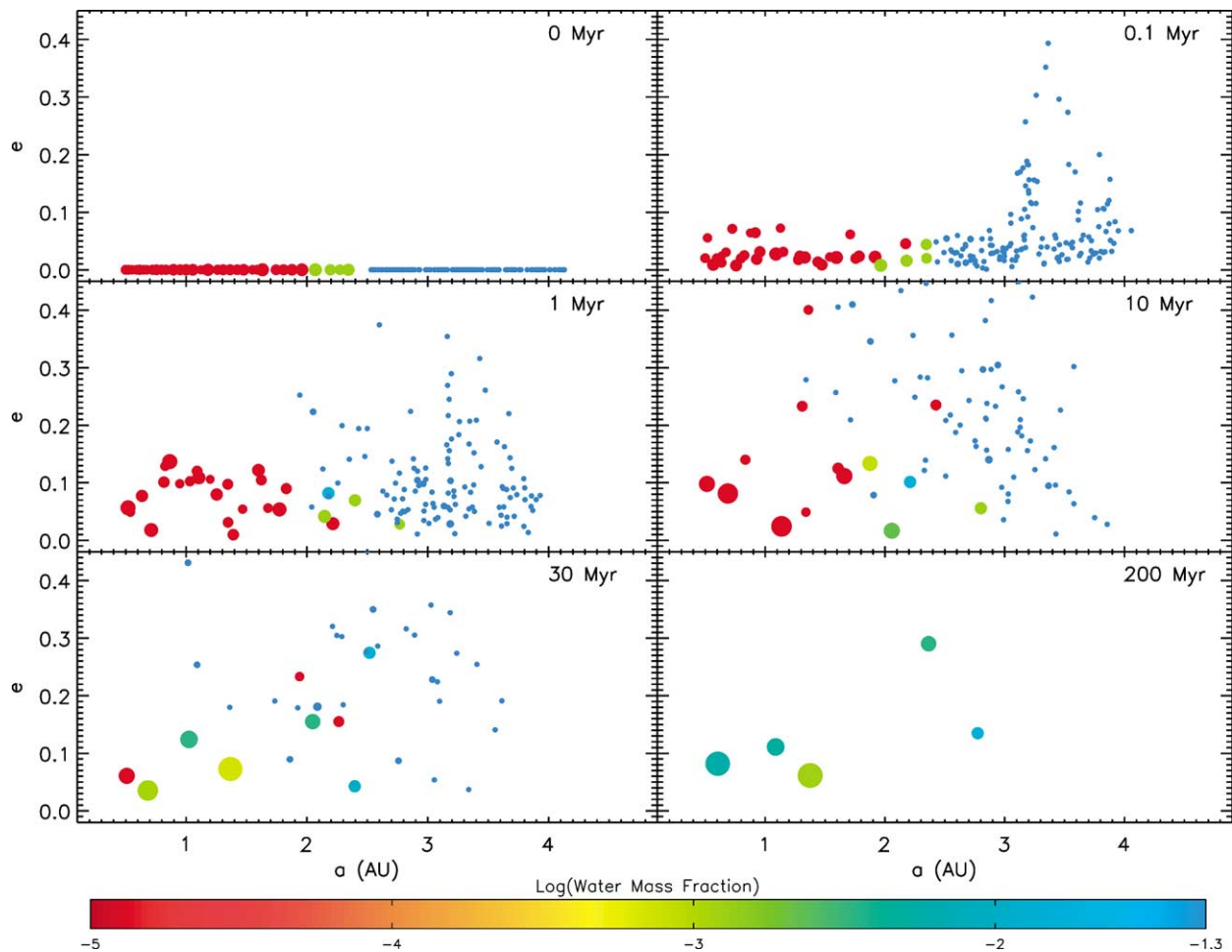


Fig. 3. Snapshots in the evolution of a simulation with Jupiter at 5.2 AU with zero eccentricity, and a planetesimal mass of $0.01M_{\oplus}$ (simulation 10: see Table 1 for details). The size of each object is proportional to its mass^(1/3) (but does not represent the actual physical size), and the color of each object corresponds to its water mass fraction. Note that the wettest objects have water mass fractions of $\log_{10}(5\%) = -1.3$. See text for discussion.

tions were run on desktop PCs, each taking roughly 1 month of CPU time on a 700 MHz machine. The three simulations with $M_J = 10M_{\oplus}$ each required 4–6 months of CPU time.

3. Results

In this section we first discuss the details of one simulation, describing the physical processes which apply to all of our simulations. We then show the dependences of the terrestrial planets we form on planetary system parameters, and statistically examine the terrestrial planets which have formed. We then address the issues of water content and habitability.

3.1. One simulation

Figure 3 shows six snapshots in time of the evolution of one simulation (simulation 10; see Table 1) with $a_J = 5.2$ AU, $e_J = 0$, $M_J = M_{J,r}$, and $0.01M_{\oplus}$ planetesimals. As

mentioned in Section 2.2, we assume that objects are dry (0.001% water) if they form interior to 2 AU, wet (5% water) if they form exterior to 2.5 AU, and moderately wet (0.1% water) in between. These compositional constraints are reflected in the initial conditions of Fig. 3.

Jupiter begins to excite the eccentricities of planetesimals in the asteroid belt, especially those which are located close to mean motion resonances. The 0.1 Myr snapshot in Fig. 3 clearly shows the 2 : 1 resonance at 3.28 AU, the 3 : 2 resonance at 3.97 AU, and a hint of the 5 : 3 resonance at 3.7 AU. Meanwhile, the planetary embryos' eccentricities are being excited to a smaller degree by their mutual gravitational pulls. As the eccentricities of planetesimals increases, their orbits become crossing, and the probability of a collision or a close encounter with Jupiter increases. A collision occurs when one is at perihelion and the other is at aphelion. The alignment of their velocities implies that a collision tends to circularize the orbit of the remaining agglomeration. Therefore, there are two likely end states for a planetesimal in resonance with Jupiter:

- (i) The planetesimal will collide with an object with a smaller semimajor axis, effectively moving the planetesimal closer to the Sun, outside of the resonance with Jupiter.
- (ii) The planetesimal's eccentricity increases to the point where it will have a close encounter with Jupiter and likely be ejected from the system.

By $t = 1$ Myr in Fig. 3 radial mixing has begun at the boundary between the dry planetary embryos and the wet planetesimals. Over the next 10 Myr planetary embryos accrete to form larger protoplanets, as planetesimals slowly diffuse inside 2 AU. Between 10 and 30 Myr, most protoplanets have accreted some material from past the snow line. At the end of the simulation ($t = 200$ Myr), three terrestrial planets have been formed inside 2 AU, and two smaller bodies reside in the asteroid belt. No planetesimals remain in the asteroid belt. Each surviving body contains a mixture of dry and wet material, to varying degrees. The eccentricities of the planets is ~ 0.1 inside 2 AU, and larger for the asteroidal planets. Two roughly Earth mass planets have formed, one inside and one outside 1 AU. One planet has formed in the habitable zone, at 1.08 AU, but is significantly less massive at $0.4M_{\oplus}$, and has a relatively high eccentricity of 0.1, whereas the more massive planets have slightly smaller eccentricities. The exact parameters of the surviving planets for all simulations are listed in Table 1.

For each of the five surviving planets from simulation 10, Fig. 4 shows the origin of every planetary embryo and planetesimal which was accreted by that planet. The dashed line indicates where the starting and final semimajor axes are equal. An object close to the dashed line had little radial displacement through the formation process, whereas an

object far from the dashed line exhibited a large radial excursion (e.g., the planetesimals from past 3 AU which were accreted by the planet at 0.6 AU). Each of the planets inside 2 AU was formed from objects throughout the inner Solar System, including at least two planetesimals from the outer asteroid belt, although the majority of their mass came from local planetary embryos. Interestingly, the planet at 1.08 AU formed entirely from material exterior to its final position. The two planets in the asteroid belt exhibit a narrower zone of accretion, but are still made up of material from different regions.

Figure 5 shows the masses of the planets from simulation 10 as a function of time, labeled by their final semimajor axes. The three planets inside 2 AU are included, as well as the inner of the two asteroid belt planets. The planets reach half of their final masses within the first 10–20 Myr, although significant accretion events occur as late as 100 Myr. There is a constraint for our own Solar System from measured Hf–W ratios that both the Moon and the Earth's core were formed by $t \simeq 30$ Myr (Kleine et al., 2002; Yin et al., 2002). This implies that the Earth's mass was within a factor of 2 of its current mass at that time. Simulation 10 satisfies this constraint. This will be discussed more generally in Section 4.

3.2. Dependences on system parameters

In all cases we form 1–4 terrestrial planets with masses from 0.23 to $3.85M_{\oplus}$, which vary in orbital parameters and volatile content. We define a terrestrial planet as a surviving body residing inside 2 AU, with a mass greater than $0.2M_{\oplus}$. There is a large variation among the planetary systems which are formed, as well as significant stochastic variation be-

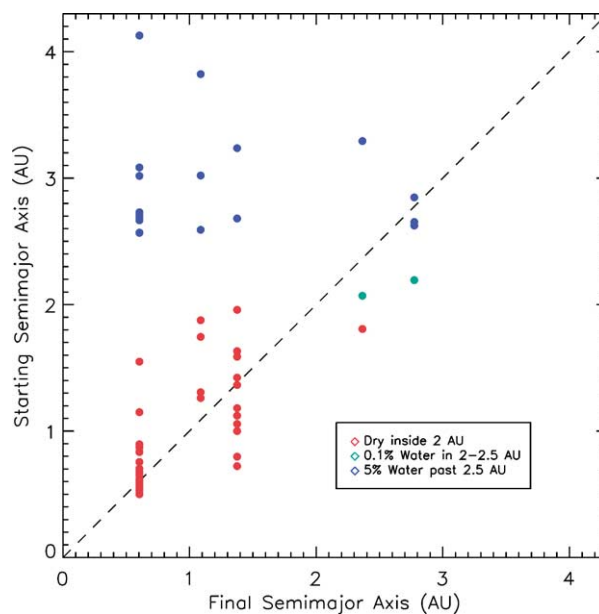


Fig. 4. Starting vs. final semimajor axes for all objects which incorporated into the five surviving bodies from Fig. 3. The dashed line is where the starting and final values are equal. See text for discussion.

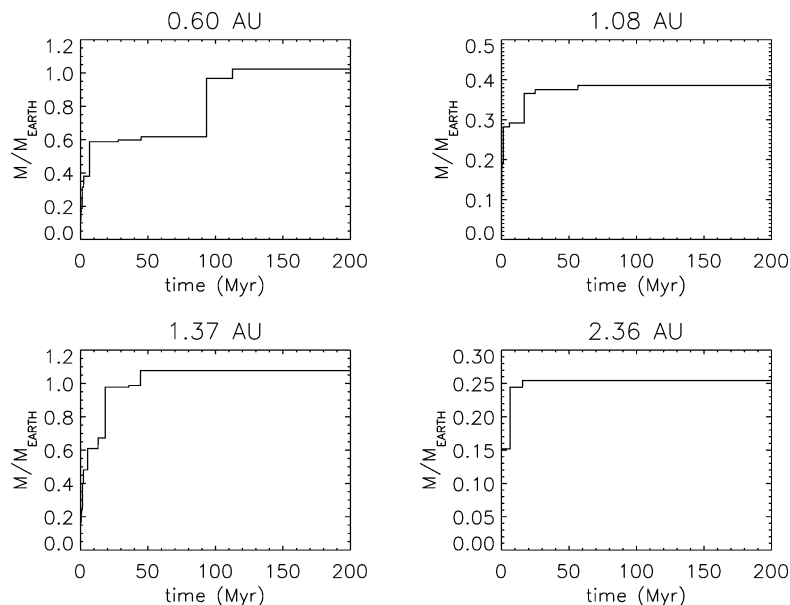


Fig. 5. Mass vs. time for objects in the simulation from Fig. 3, labeled by their final semimajor axes. The three planets inside 2 AU are included, as well as the innermost object in the asteroid belt.

tween simulations with identical parameters. We now summarize how the terrestrial planets we form are affected by planetary system parameters:

3.2.1. Planetesimal mass

The mass of a planetesimal in the outer asteroid region causes large variations in the terrestrial planets which are formed. Recall that in Section 2.1 we defined the two planetesimal masses we use in our simulations. In case (i) the total mass in the asteroid region is accounted for and the planetesimal mass is $\sim 0.1M_{\oplus}$, and in case (ii) the planetesimal mass is fixed at $0.01M_{\oplus}$. Cases (i) and (ii) can be thought of as upper and lower limits to the amount of material in solids past the snow line for a given surface density profile. Some case (i) simulations have $10\text{--}15M_{\oplus}$ in the outer asteroid area, which is roughly a factor of 2–3 larger than standard models for the solar nebula.

The (arithmetic) mean water mass fraction of the planets formed in all case (i) simulations is 1.7×10^{-2} vs. 4×10^{-3} for all case (ii) simulations. The average planet mass for case (i) is $1.8M_{\oplus}$ vs. $0.9M_{\oplus}$ for case (ii). The mean number of planets per simulation for case (i) is 2.5 vs. 3.2 for case (ii), and the total mass in terrestrial planets is $4M_{\oplus}$ for case (i) vs. $2.7M_{\oplus}$ for case (ii). The mean eccentricities of all terrestrial planets for case (i) is 0.14, vs. 0.10 for case (ii).

The fact that case (i) simulations produce more eccentric terrestrial planets than case (ii) simulations indicates a higher degree of dynamical excitation, which is expected from a more massive outer disk. The observed trends can therefore be explained with the reasoning of Levison and Agnor (2003) as follows. A system of eccentric protoplanets encounters a larger fraction of other protoplanets than a less dynamically excited system. The orbits of these eccentric bodies cover a large segment of the disk, making it

difficult for growing planets to isolate themselves dynamically from each other. This results in a larger feeding zone for each planet, and a smaller number of more massive planets in a more dynamically excited protoplanetary system. This trend is clearly seen in case (i) vs. case (ii) simulations.

3.2.2. Surface density

The effects of surface density should be similar to those of the planetesimal mass. However, since we have only covered a relatively small range in values of Σ_1 and Σ_{snow} in these simulations, the direct effects are negligible compared with the effects of the planetesimal mass and the stochastic “noise” inherent to the simulations.

3.2.3. Jupiter’s mass

A jovian planet of larger mass forms a smaller number of terrestrial planets than a lower-mass body. The masses of the terrestrial planets increase slightly with the mass of the jovian planet, but this is a small effect compared with the effects of the planetesimal mass. In our 30 case (ii) simulations, the total mass incorporated in terrestrial planets is roughly constant with M_J at $\sim 2.5M_{\oplus}$, 25% higher than in our Solar System. The water content of the terrestrial planets does not vary significantly with M_J .

The number of surviving bodies at the end of the 200 Myr integration (which includes planets and remnant planetesimals and planetary embryos) increases sharply at small Jupiter masses, with an average of 54 for a $10M_{\oplus}$ Jupiter. Since the algorithm used in Mercury, and therefore the amount of CPU time required, scales with the number of bodies, n , as n^2 , this explains the large increase in computational expense for the $10M_{\oplus}$ Jupiter simulations compared with those with a more massive gas giant.

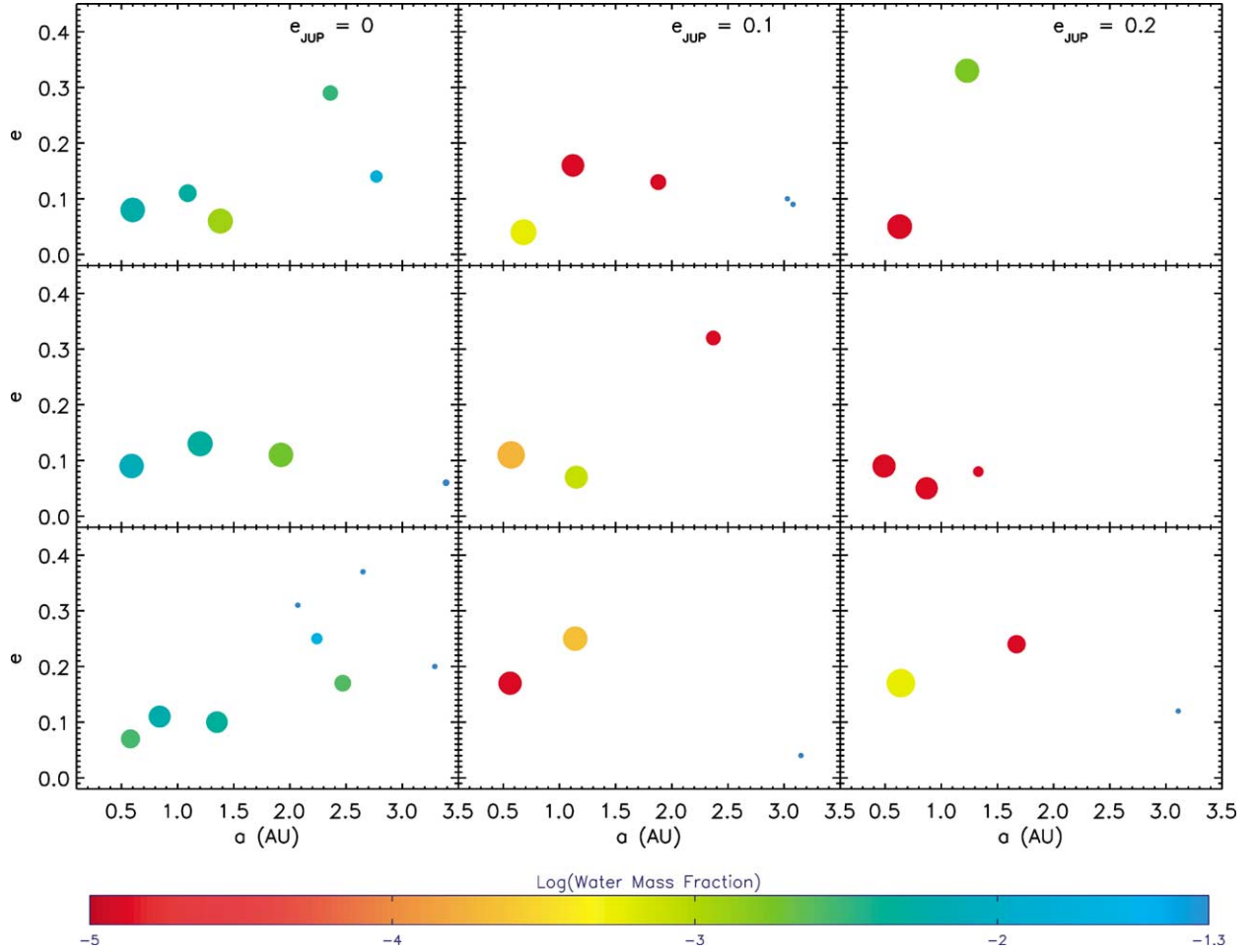


Fig. 6. The final configuration of nine planetary systems with identical initial conditions ($a_J = 5.2$ AU, $M_J = M_{J,r}$, $M_{\text{planetesimal}} = 0.01M_{\oplus}$) apart from Jupiter's initial eccentricity, which is the same for all simulations in a given column. Note the dramatic decline in volatile content for e_J greater than zero.

3.2.4. Jupiter's eccentricity

Figure 6 shows the configuration of nine planetary systems at the end of a 200 Myr integration, including three with $e_J = 0.1$ and three with $e_J = 0.2$. An eccentric Jupiter clears out the asteroid region much more quickly than a low eccentricity Jupiter, both by increased ejection efficiency and, more significantly, a large increase in the number of objects which collide with the Sun, as expected from the results of Chambers and Wetherill (2001). The result of this is that eccentric giant planets tend to form volatile-poor terrestrial planets. The mean water mass fraction of fourteen terrestrial planets which formed in the six simulations with $e_J = 0.1$ or 0.2 is 2×10^{-4} , vs. 8×10^{-3} for all simulations with $e_J = 0$. The mean total mass in terrestrial planets in these six simulations was $2.0M_{\oplus}$, as compared with $2.5M_{\oplus}$ for all case (ii) simulations with $e_J = 0$. The terrestrial planets in these simulations have higher average eccentricities than those with $e_J = 0$ (0.14 vs. 0.10). Also, in five out of these six simulations the most massive terrestrial planet which formed was the innermost, which is consistent with the results of Levison and Agnor (2003). The explanation for this is again due to a large amount of dynamical excitation due to Jupiter,

which increases the eccentricities of protoplanets and makes it easier for planets to form close to the central star. Mechanisms for dynamical excitation are discussed below.

To first order, the effective width of a Jupiter mean motion resonance scales with Jupiter's eccentricity as $\delta a/a \propto e_J^{1/2}$ (Murray and Dermott, 2001, Eq. (8.76)). This is a simplification, as the phase space structure of resonances is quite complex. More importantly, the secular excitation felt by bodies in the terrestrial region due to an eccentric Jupiter is increased, with maximum eccentricity of an excited massless body $e_{\text{max}} \propto e_J$ and a time to reach e_{max} of $\tau \propto a^2$ (Levison and Agnor, 2003). A combination of these strong secular and resonant effects will act quickly in the outer asteroid region, due to stronger secular forcing and the large number of mean motion resonances. This explains the much more rapid depletion of the asteroid belt in the case of an eccentric Jupiter, resulting in volatile-poor terrestrial planets. Note that secular resonances due to the precession of Jupiter's orbit would be induced if an additional giant planet (e.g., Saturn) were included in the simulations.

Jupiter's eccentricity does not remain constant throughout the integrations. In the six simulations with an initially

eccentric Jupiter, the eccentricity was damped by an average of 0.02 after 200 Myr, while ejecting roughly 2 Earth masses worth of planetesimals and embryos from the system. Jupiter’s semimajor axis decreased by an average of 0.04 AU in these six simulations. These numbers are similar to the results of Chambers and Wetherill (2001).

3.2.5. *Jupiter’s semimajor axis*

We see a weak correlation between higher water content in terrestrial planets and Jupiter’s semimajor axis. In the case of a Jupiter at 4 AU, there is simply a smaller reservoir of volatile-rich material between the snow line and Jupiter as compared with a system with $a_J = 5.2$ AU, resulting in drier planets. In the case of a Jupiter at 7 AU, this reservoir is much larger. However, as Jupiter’s zone of influence is at larger heliocentric distances, there is a larger change in energy required to deliver volatile-rich planetesimals to the terrestrial region. In addition, the super embryos which form between the snow line and the 3 : 1 Jupiter resonance have relatively large feeding zones, and present an obstacle for inward-bound planetesimals. As a result, the innermost terrestrial planet is completely dry in four out of seven simulations with $a_J = 7$ AU, and the mean water mass fraction of all planets formed inside 1 AU is 1.7×10^{-3} , and 3.8×10^{-2} for planets which formed between 1 and 2 AU. This is not unexpected, as super embryos immediately past the snow line at 2.5 AU can act as accretion seeds and occasionally migrate inside 2 AU, resulting in massive (1.5 to $3 + M_{\oplus}$) planets in the proximity of Mars’ current orbit.

Jupiter’s semimajor axis decreases slowly with time in all simulations, as it ejects planetesimal material from the Solar System, and the magnitude of this effect changes with planetesimal mass. For all case (i) simulations the mean change in Jupiter’s semimajor axis was 5% ($\delta a \sim 0.03$ AU for $a_J = 5.2$ AU), compared with 2% for all case (ii) simulations ($\delta a \sim 0.01$ AU for $a_J = 5.2$ AU). We started Jupiter’s orbit at 5.5 AU in 9 simulations, in an attempt to match Jupiter’s final semimajor axis of 5.2 AU. In three of these cases Jupiter’s mass was only $10M_{\oplus}$, and Jupiter’s final semimajor axis was about 5 AU in each case. In the six other cases Jupiter typically migrated 0.05–0.15 AU, ending up at roughly 5.4 AU.

3.2.6. *The position of the snow line*

The most important consequence of a snow line at 2 AU rather than 2.5 AU is that it lies inside the 3 : 1 resonance with a Jupiter at 5.2 AU, resulting in the formation of super embryos in the annulus between 2 and 2.5 AU. As mentioned above, these can act as an obstacle to inward-diffusing planetesimals. However, in four simulations with the snow line at 2 AU we see little difference in the terrestrial planets. The two simulations with a snow line at 5 AU form relatively water-rich planets, but no trends are clear between these and other case (i) simulations with higher-mass planetesimals. We intend to explore this region of parameter space in more detail in future work.

3.2.7. *Time of Jupiter formation*

We see no significant physical differences between the terrestrial planets in simulations with a $10M_{\oplus}$ Jupiter seed which grew to full size at 10 Myr and those which began with a full size Jupiter. More simulations are needed to overcome stochastic noise and small number statistics, in order to establish correlations.

3.3. *Water content*

Table 2 summarizes the results of the water added to terrestrial planets within a semimajor axis range of 0.8–1.5 AU from the parent star. This is larger than the so-called “continuously habitable zone” (CHZ) defined as the semimajor axis realm for which a planet’s mean surface temperature will be above the water melting point, but not so high as to allow loss of water by evaporation and subsequent photolysis (Kasting et al., 1993; Kasting, 1988). The CHZ could be as narrow as 0.05–0.1 AU centered on the Earth’s orbit, but this could be too narrow or too wide given our lack of knowledge regarding the range of habitable planetary environments and the robustness of processes that buffer stable liquid water environments on planets. A better constraint would be the search space planned for the Terrestrial Planet Finder (NASA) and Darwin (ESA) programs designed to detect and characterize Earths around other stars (see part 4). This search space, for a solar-mass star such as that which we are considering here, ranges from 1.5 AU (the orbit of Mars in our Solar System) to as close as 0.7 AU (Venus’ orbit).

All but a few of our simulations generate planets within the semimajor axis space 0.8–1.5 AU (Table 2), and these planets acquire a wide range of water during their buildup from lunar-to-Mars-sized bodies as simulated in this paper. A useful absolute unit of water content is an “Earth ocean,” defined to be 1.5×10^{24} g of water. This is the amount of water in the hydrosphere (oceans, rivers, lakes, etc.) of the Earth today, excluding an additional 15% in the crust of our planet. Highly uncertain is how much additional water is in the Earth’s deep interior today—estimates range from much less than 1 Earth ocean to several Earth oceans (Abe et al., 2000). The amount present during accretion of the Earth is even more poorly constrained, because of a lack of geochemical evidence for the extent of hydration of the primitive mantle. Some geochemists argue that the Earth possessed large amounts (> 10 Earth oceans) of water (Dreibus and Wanke, 1989), but others assert that the current inventory is close to the total quantity accreted.

The amount of water accreted by our modeled terrestrial planets, in the 0.9–1.5 AU region, ranges from 0 to almost 300 Earth oceans. These numbers should be decreased to account for loss of water during the large embryo impacts that characterize the growth of the terrestrial planets in our simulations. The fraction of volatiles lost during a large collision is uncertain. Recent results (Melosh, 2003, and references therein) suggest that only 30% of the Earth’s atmosphere was lost during the Moon-forming collision, in-

Table 2
 “Habitable” planets with $0.8 \text{ AU} < a < 1.5 \text{ AU}$ (**$0.9 \text{ AU} < a < 1.1 \text{ AU}$**)^a

Simulation	a (AU)	e	i (deg)	Mass (M_{\oplus})	N (oceans) ^b	WMF ^c
1	1.09	0.11	4.1	2.02	53	6.7×10^{-3}
2	0.98	0.15	19.3	0.86	0	1.0×10^{-5}
3	1.24	0.10	2.7	2.03	35	4.4×10^{-3}
4	1.15	0.08	7.7	1.28	36	7.1×10^{-3}
5	1.40	0.25	9.5	0.96	91	2.4×10^{-2}
10a	1.09	0.11	8.1	0.38	5	3.9×10^{-3}
10b	1.38	0.06	1.4	1.08	3	9.3×10^{-4}
11	1.20	0.13	6.5	1.09	16	3.8×10^{-3}
12a	0.84	0.11	6.3	0.74	14	4.8×10^{-3}
12b	1.35	0.10	5.0	0.70	9	3.6×10^{-3}
13	1.00	0.02	4.5	1.27	13	2.6×10^{-3}
14	1.43	0.07	1.5	1.94	297	3.8×10^{-2}
15	1.43	0.06	14.9	1.17	183	3.9×10^{-2}
16	1.43	0.04	8.3	1.14	4	9.3×10^{-4}
17a	1.01	0.03	1.8	0.61	6	2.5×10^{-3}
17b	1.43	0.00	3.5	0.62	4	1.8×10^{-3}
19a	1.00	0.17	6.8	0.71	8	2.9×10^{-3}
19b	1.44	0.10	4.3	1.02	17	4.4×10^{-3}
20	1.48	0.10	1.6	2.82	322	2.9×10^{-2}
21	1.26	0.10	14.3	1.08	154	3.6×10^{-2}
22	0.92	0.03	3.7	1.25	27	5.6×10^{-3}
23a	0.84	0.05	0.7	0.96	11	3.1×10^{-3}
23b	1.36	0.10	1.4	0.86	11	3.5×10^{-3}
24	1.32	0.16	7.8	1.77	215	3.1×10^{-2}
25	1.05	0.07	5.8	3.11	292	2.4×10^{-2}
26	1.33	0.07	5.1	1.54	13	2.1×10^{-3}
27	1.21	0.06	5.9	1.07	26	6.2×10^{-3}
28	0.96	0.14	5.1	3.85	352	2.3×10^{-2}
29	1.34	0.16	2.0	2.05	254	3.1×10^{-2}
30	1.12	0.16	2.8	0.80	0	1.0×10^{-5}
31	1.15	0.07	7.4	0.84	1	6.0×10^{-4}
32	1.14	0.25	4.1	1.01	0	1.5×10^{-4}
33	1.23	0.33	7.8	0.98	5	1.3×10^{-3}
34	0.87	0.05	10.5	0.77	0	1.0×10^{-5}
37	0.85	0.04	12.6	0.77	5	1.9×10^{-3}
38a	0.97	0.02	7.6	1.31	7	1.5×10^{-3}
38b	1.45	0.06	6.3	0.30	1	1.6×10^{-3}
39	1.15	0.02	1.6	1.75	23	3.3×10^{-3}
40	1.12	0.05	2.3	1.13	13	3.1×10^{-3}
41a	0.87	0.02	2.6	0.80	5	1.9×10^{-3}
41b	1.16	0.04	5.8	0.54	5	2.8×10^{-3}
42a	0.91	0.01	4.3	0.97	3	1.0×10^{-3}
42b	1.40	0.09	4.2	0.61	12	5.1×10^{-3}
43	1.39	0.12	13.5	0.73	41	1.39×10^{-2}
44	1.24	0.15	7.1	1.33	61	1.15×10^{-2}
Earth^d	1.00	0.03	2.1	1.00	~1–10	1.0×10^{-3}

^a Planets with $0.9 \text{ AU} < a < 1.1 \text{ AU}$ are shown in bold, and depicted in Fig. 8.

^b Number of oceans of water accreted by the terrestrial planet, where an ocean is equal to 1.5×10^{24} grams of water.

^c Water Mass Fraction of the planet.

^d The orbital elements for the Earth are 3 Myr averages from Quinn et al. (1991). The water content of Earth’s mantle is uncertain. We assumed the Earth’s total water budget to be four oceans in calculating the water mass fraction. See Morbidelli et al. (2000) for a discussion.

dicating that the water contents of our modeled planets are realistic to within roughly a factor of two, and vary with the number of large collisions during the formation of each planet. Even so, some planets clearly receive much more water than did the Earth during its formation, and some ended up essentially dry (those with a value zero might

have some trace amounts of water depending on the water content of 1 AU planetesimals; see below). There is no correlation in our simulations between the amount of water acquired and other parameters such as final planet mass, orbit, or positions and mass of the giant planet in the simulation. The number of bodies from beyond 2–2.5 AU that

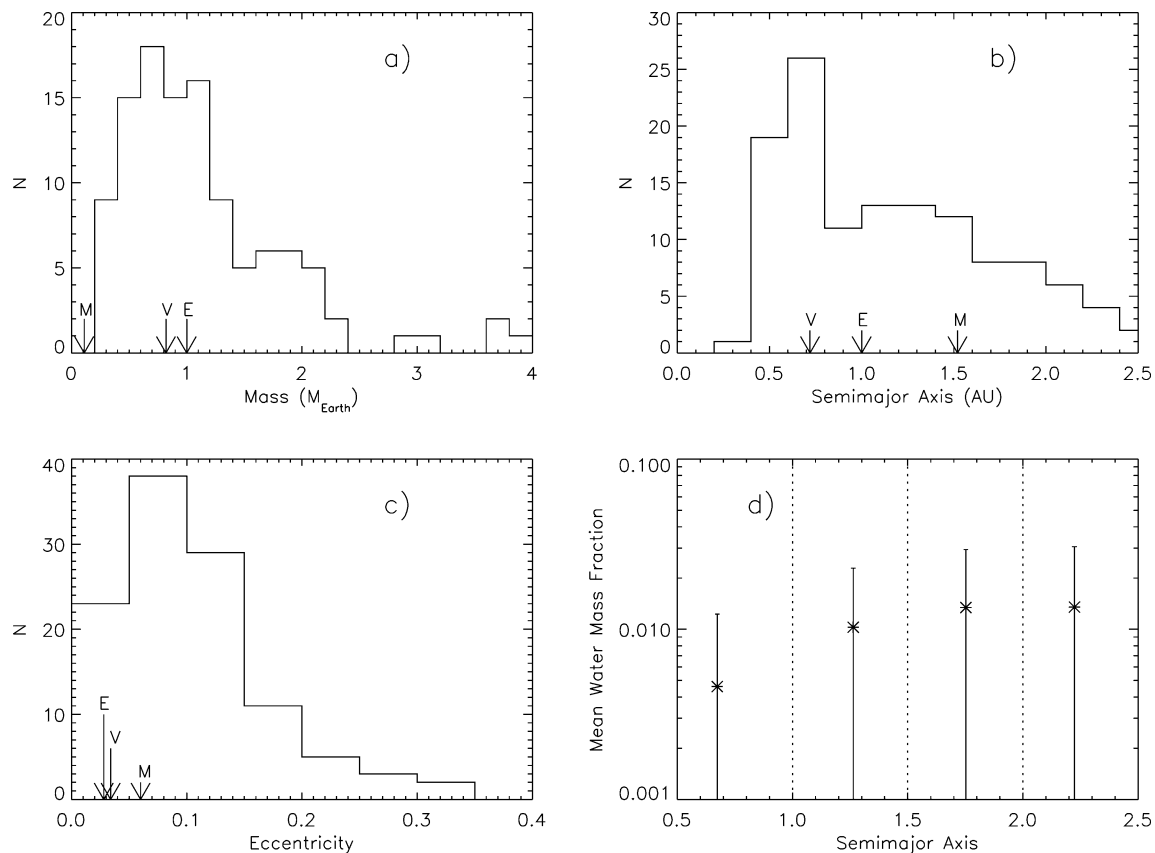


Fig. 7. Orbital and physical characteristics of 111 terrestrial planets formed in 44 simulations, and 12 planets which formed between 2 and 2.5 AU. Panels (a)–(c) show mass, eccentricity and semimajor axis functions. Values for Venus, Earth, and Mars are labeled with arrows which correspond to their values averaged over a 3 Myr integration (Quinn et al., 1991). Panels (a) and (b) are comprised solely of the planets inside 2 AU. Panel (d) shows the mean water content of terrestrial planets as a function of their final semimajor axis, divided into four zones as indicated by the dotted vertical lines, with one sigma error bars. The statistical significance of panels (c) and (d) is discussed in the text.

end up in the 0.9–1.5 AU region is highly sensitive to the initial conditions, and they determine the water delivered to the growing terrestrial planets. The results reflect well the stochastic nature of the accretion process in a planet-forming environment stirred up dynamically by jovian-mass bodies.

Some cosmochemists have argued that the planetesimals in the region of 1 AU, where the Earth formed, were not dry but instead had as much water as was required to produce what is seen in the Earth today (Drake and Righter, 2002). The geochemical arguments regarding a local versus distal source of water are too involved to get into here (Robert, 2001). Were we to assume that material at 1 AU possesses, let us say for sake of argument, 0.05% water (2 Earth oceans), then our results would reflect somewhat larger amounts of water than are shown in Table 2. But the amount of water in the carbonaceous chondrites is so large that the shift would not be substantial, except that the driest planets would have at least 2 Earth oceans rather than 0. The stochasticity of the results would be preserved, reflecting the chance delivery of large bodies from the region beyond 2.5 AU that is one of the signatures of terrestrial planet accretion according to this model.

3.4. Characterizing the formed terrestrial planets

We have formed a total of 111 terrestrial planets in 44 simulations. (Recall our definition that a terrestrial planet has $a < 2$ AU and $M > 0.2M_{\oplus}$.) This ensemble is comprised of planets which formed in a wide range of environments, and is more suited to examining the possible outcomes of planet formation rather than the likely outcomes in specific cases or the true distributions of terrestrial planets in our galaxy.

Figure 7 summarizes the physical properties of these 111 terrestrial planets. Panels (a), (b), and (c) give the mass, semimajor axis and eccentricity functions, respectively, of our sample. Panel (a) shows that one Earth mass is not an upper limit to the mass of terrestrial planets, which can have masses up to 3–4 M_{\oplus} . Panel (b) demonstrates that we form terrestrial planets throughout the terrestrial region, with the innermost planet forming at 0.34 AU. Recall, however, that our initial conditions start with planetary embryos at 0.5 AU due to computational constraints.

Panel (c) shows the eccentricity distribution of terrestrial planets (inside 2 AU). We performed a one-sided Kolmogorov Smirnov test to see if the planets in our Solar System are consistent with having been drawn from this ec-

centricity function. If we consider only Earth, Venus, and Mars, then the Solar System does not match this distribution to 95% confidence (90% if only simulations with $m_{\text{planetesimal}} = 0.01M_{\oplus}$ —case (ii) above—are considered). If Mercury is included, then the statistic is insignificant, as the Solar System is inconsistent with the distribution with 74% confidence (53% for case (ii) only). This is not a new problem, as many authors (e.g., Chambers, 2001, 2003) have had trouble matching the low eccentricities and inclinations in our Solar System to numerically formed terrestrial planets. The answer may lie in including the damping effects of small bodies (i.e., dynamical friction), which are present as planetesimals in the protoplanetary disk, as well as being repopulated as impact fragments. It is unlikely that gas drag plays a role in the damping, as all gas is expected to be gone from the system by 10 Myr (Briceño et al., 2001).

Panel (d) shows the radial variation in water content of these planets, divided into four semimajor axis bins:

- (1) $a < 1$ AU,
- (2) $1 \text{ AU} < a < 1.5$ AU,
- (3) $1.5 \text{ AU} < a < 2$ AU, and
- (4) $2 \text{ AU} < a < 2.5$ AU.

We performed a Wilcoxon test on each two adjacent bins to test whether the difference in water content of the planets in these bins is statistically significant. We found that the difference between bins 1 and 2 was significant to 99.6%, but that there is no statistical difference between the means in bins 2, 3, and 4. If we only include simulations with $m_{\text{planetesimal}} = 0.01M_{\oplus}$ (case (ii) above), the difference between bins 1 and 2 is still significant to 99.4%, and there remains no difference between the outer three bins.

4. Discussion

In 44 simulations, we have formed terrestrial planetary systems of all shapes and sizes, with 1–4 terrestrial planets and a range in water content and orbital characteristics. The extremes are systems in which only one, very massive terrestrial planet has formed (e.g., simulation 28: see Fig. 8) and systems which have many, lower-mass, more closely packed systems with 4 planets inside 2 AU (e.g., simulation 42: see Fig. 8). These results imply the existence of a huge variety of planetary systems in our galaxy, as planets form from disks around stars with a variety of masses and metallicities.

Chambers (2003) formed “life-sustaining” planets in his simulations, defined to be in the habitable zone with water mass fractions greater than 4×10^{-4} . He found that the water content of terrestrial planets depends strongly on the eccentricity, mass and formation time of the giant planets, with larger values of e_J and M_J leading to drier planets, while larger values of t_J led to more volatile-rich planets. He also found that systems with lower mass giant planets form the most life-sustaining planets.

Our results are partially consistent with Chambers’. We also find that e_J plays a large role in terms of the water content of terrestrial planets, and two of the 11 “habitable” planets we formed between 0.9 and 1.1 AU were from only four simulations with $M_J = \frac{1}{3}M_{J,r}$, and both had enough water to be deemed “life-sustaining.” However, we see no correlation between Jupiter’s mass and the water content of terrestrial planets. This could be due to our relatively small number of simulations. We have not performed enough simulations with different values of t_J to reach a reliable conclusion.

4.1. Applications to TPF/Darwin

TPF and Darwin are respectively, US and European projects to put large telescopic systems into space to detect and spectroscopically characterize Earth-sized planets around other stars, with the goal of identifying those with spectroscopic signatures suggesting habitability (water) or even life (molecular oxygen) (Beichman et al., 1999). While efforts are being made to design the systems to detect Earths in as broad a range of semimajor axes as possible, detection of an Earth-sized planet in a Venus-like orbit at 0.7 AU from a solar-type star may pose special problems in nulling-out or blocking the light of the parent star. However, the results we show in Table 2 suggest that there will be many such candidates in Venus-like orbits, and hence a complete census of terrestrial planets in Venus-to-Mars-sized orbits remains a desirable goal.

Most significant among our results is the robustness of terrestrial planet formation. This has been shown previously for starting positions of the giant planets akin to our Solar System (Chambers and Cassen, 2002), and we have extended the results by including giant planets over a wide range of masses and a range of orbits commensurate with terrestrial planet stability but varying significantly from the Solar System situation. While terrestrial planet formation—that part of the process in which lunar-to-Mars-sized bodies are cleaned up to form a few Earth-sized planets—is stochastic, it still leads to planets familiar to us in terms of size and position. Of course, one can start with initial conditions so different from our Solar System that predominantly smaller or larger planets result, and indeed if residual nebular gas is included in the simulation, numerous Mars size bodies replace the handful of Earth-size objects (Kominami and Ida, 2002). But in the coarse view, it seems easy to make terrestrial planets and hence the TPF/Darwin projects ought to assume a high likelihood of terrestrial planets around solar-type stars for which giant planets are not so close as to induce orbital instability.

Our results also predict, as discussed above, a wide range of possible water abundances, which we summarize in Fig. 9. “Mars-like” worlds have less than an Earth ocean of water (Lunine et al., 2003). “Water-rich” worlds may be so wet as to have a geologic evolution different from ours; “water worlds” are dominated by deep water mantles and remain speculative (Leger et al., 2004).

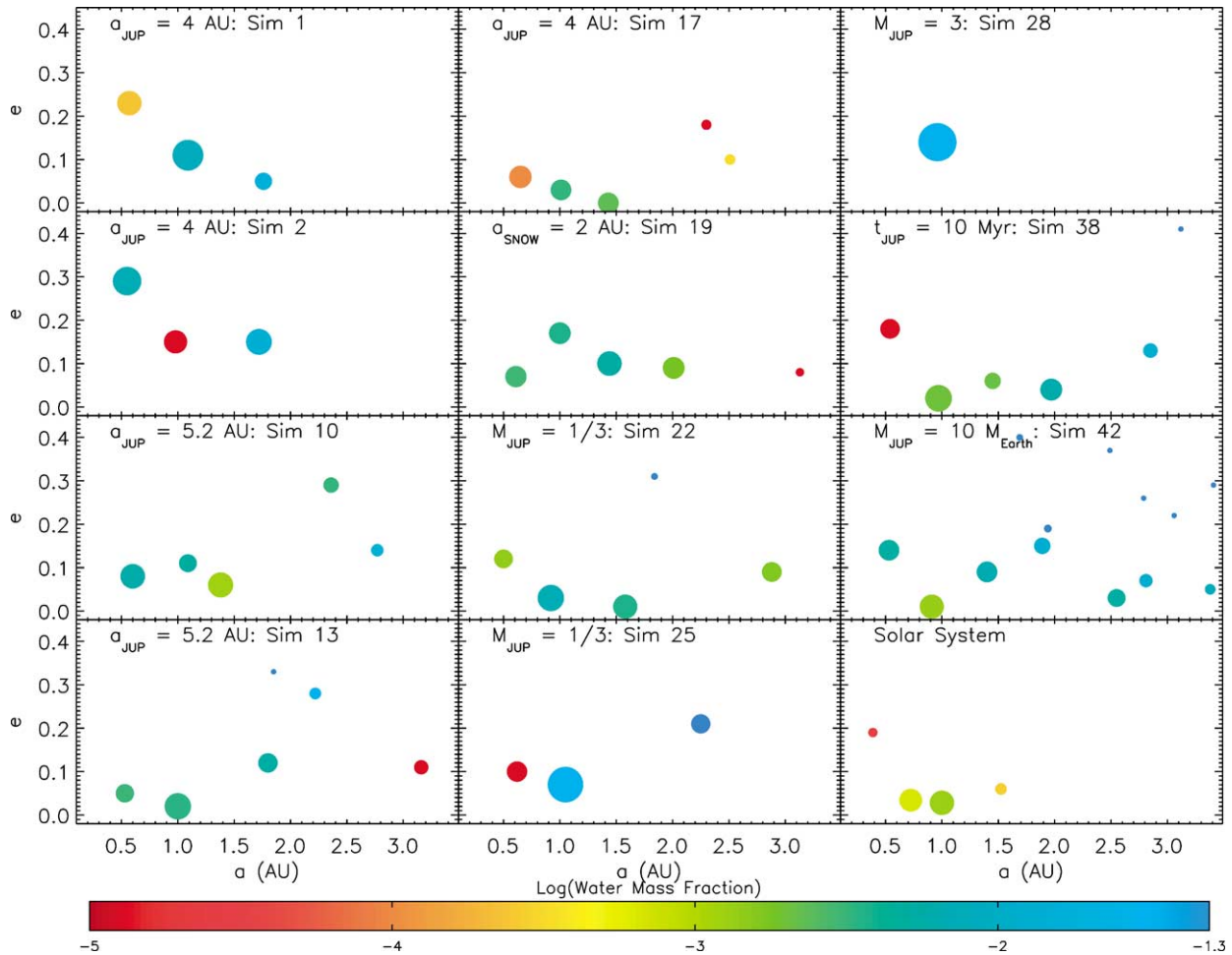


Fig. 8. Final configuration of 11 simulations which formed a “habitable” planet with $0.9 \text{ AU} < a < 1.1 \text{ AU}$, labeled by the physical parameters of each planetary system and the simulation number. If not otherwise mentioned, $M_J = M_{J,r}$ and $e_J = 0$. Our Solar System is included for comparison, with 3 Myr averaged values from Quinn et al. (1991). See Tables 1 and 2 for more details.

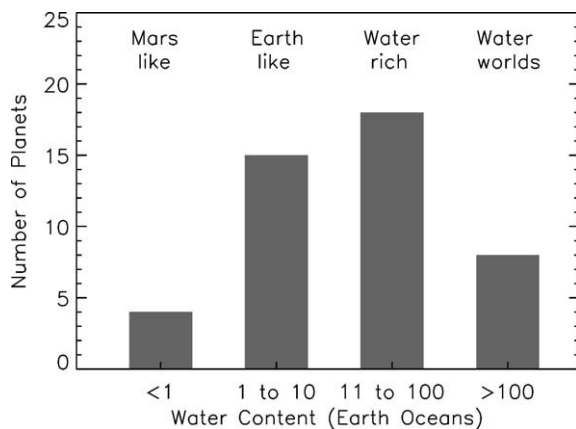


Fig. 9. Histogram of the water content of 45 planets with $0.8 \text{ AU} < a < 1.5 \text{ AU}$ which formed in 44 simulations. See text for discussion.

We do not believe our sample of initial conditions to be a representative sample of possible scenarios in the galaxy, but rather a test of certain key parameters which are important

to the process of terrestrial planet formation. In addition, the majority of the planets in Table 2 have water contents within an order of magnitude of that of the Earth (only 11 planets have more than 50 oceans). With the uncertainty in both volatile retention during the formation process as well as the snow line’s position, we conclude that Earth-like planets are likely to be relatively common in the galaxy. We caution the reader that we do not believe our results to indicate a preponderance of “water worlds” in the galaxy. At this stage we are unable to make accurate statistical claims as to the precise quantitative nature of extrasolar terrestrial planets. We do, however, believe our results to show the variety of possible terrestrial planets, including extremes which are now being seriously considered (e.g., Leger et al., 2004).

The spectroscopic signature of water vapor in an atmosphere is such as to be an insensitive diagnostic of water abundance—other than indicating that indeed surface water is present and surface temperatures warm enough for significant water vapor. Yet, the bulk water abundance will certainly affect the evolution of a planet, in terms of tectonic styles (e.g., plate tectonics on Earth versus dominant

basaltic volcanism on Venus), hence cycling of volatiles, and other processes that in complex ways determine habitability. Modeling such planets provides a perspective on these dependencies, but as yet unknown is how to remotely assess another Earth as nearly dry or so rich in water as to be a novel, “water-world” terrestrial planet. Our results suggest that both ends of the spectrum must be seriously considered.

5. Conclusions

We have performed 44 simulations of terrestrial planet formation, with initial conditions designed to reflect the state of the protoplanetary disk at the end of oligarchic growth (see Table 1). These simulations produced a variety of planetary systems. Planets formed with masses from $0.23M_{\oplus}$ to $3.85M_{\oplus}$, and with water contents ranging from completely dry to “water worlds” with 300+ oceans of water. A total of 43 planets formed between 0.8 and 1.5 AU, including 11 “habitable” planets between 0.9 and 1.1 AU (see Table 2 and Fig. 8).

Terrestrial planet formation is a robust process, and a stochastic one. Stochastic “noise” between simulations with similar initial conditions made it difficult to spot trends with certain parameters. We found that the parameter with the strongest effect on the terrestrial planets was the planetesimal mass we chose, reflecting the surface density past the snow line. A high density (and large planetesimal mass) in this region results in the formation of a smaller number of terrestrial planets with larger masses and higher water content, as compared with planets which form in systems with lower densities past the snow line (and smaller planetesimal masses).

Jupiter’s eccentricity plays an important role in the volatile delivery process, as even a modest eccentricity of 0.1 drastically reduces the water content of the terrestrial planets. Systems with $e_J > 0$ tend to form terrestrial planets with slightly higher eccentricities than those with $e_J = 0$, and the total mass in terrestrial planets is less for systems with eccentric Jupiters. This is significant in light of the high eccentricities of discovered extrasolar planets.

In the cases of Jupiter at 7 AU, or a snow line of 2 AU and Jupiter at 5.2 or 7 AU, our model predicts the formation of 1– $2M_{\oplus}$ “super embryos,” protoplanets which form in a region of enhanced density between the snow line and 3 : 1 Jupiter resonance. These super embryos serve as a small dynamical barrier for inward-diffusing, volatile-rich planetesimals. This is reflected in the very low mean water content of the innermost terrestrial planet in systems with $a_J = 7$ AU. Super embryos can also serve as the accretion seed for massive terrestrial planets with high water contents.

We believe our sample to be representative of the extremes of terrestrial planet formation under our assumed initial conditions (i.e., what is possible), rather than to be characteristic of the planets in our galaxy. It is unclear at the present which initial conditions are the most realistic.

In future work we intend to improve the resolution of these simulations by increasing the number of particles by an order of magnitude. We will probe new regions in parameter space, in order to further improve our understanding of how terrestrial and habitable planets form.

Acknowledgments

We thank referees John Chambers and Junko Kominami, and editor Alessandro Morbidelli for helping us to improve the manuscript. J.L. is grateful to the NASA Planetary Atmospheres program for support. S.R. and T.Q. are grateful to the NASA Astrobiology Institute for support. Many of the simulations presented here were performed on computers graciously donated by Intel. S.R. thanks John Chambers for the use of his code (Mercury) and insightful discussions, and Don Brownlee and Monika Kress for many constructive conversations.

References

- Abe, Y., Ohtani, E., Okuchi, T., Righter, K., Drake, M., 2000. Water in the early Earth. In: Righter, K., Canup, R. (Eds.), *Origin of the Earth and the Moon*. Univ. of Arizona Press, Tucson, pp. 413–433.
- Balsiger, H., Altwegg, K., Geiss, J., 1995. D/H and O-18/O-16 ratio in the hydronium ion and in neutral water from in situ ion measurements in Comet Halley. *J. Geophys. Res.* 100, 5827–5834.
- Beichman, C., Woolf, N.J., Lindensmith, C.A., 1999. The terrestrial planet finder. Washington, DC, NASA Headquarters. Ref Type: Report.
- Bell, K.R., Cassen, P.M., Klahr, H.H., Henning, T., 1997. The structure and appearance of protostellar accretion disks: limits on disk flaring. *Astrophys. J.* 486, 372–387.
- Bell, K.R., Cassen, P.M., Wasson, J.T., 2000. The FU orionis phenomenon and solar nebula material. In: Mannings, V., Boss, A.P., Russell, S.S. (Eds.), *Protostars and Planets IV*. Univ. of Arizona Press, Tucson, pp. 897–926.
- Bockelee-Morvan, D., Gautier, D., Lis, D.C., Young, K., Keene, J., Phillips, T., Owen, T., Crovisier, J., Goldsmith, P.F., Bergin, E.A., Despois, D., Wooten, A., 1998. Deuterated water in Comet C/1996 B2 (Hyakutake) and its implications for the origin of comets. *Icarus* 133, 147–162.
- Briceño, C., Vivas, A.K., Calvet, N., Hartmann, L., Pacheco, R., Herrera, D., Romero, L., Berlind, P., Sanchez, G., Snyder, J.A., Andrews, P., 2001. The CIDA-QUEST large-scale survey of Orion OB1: evidence for rapid disk dissipation in a dispersed stellar population. *Science* 291, 93–97.
- Chambers, J.E., 1999. A hybrid symplectic integrator that permits close encounters between massive bodies. *Mon. Not. R. Astron. Soc.* 304, 793–799.
- Chambers, J.E., 2001. Making more terrestrial planets. *Icarus* 152, 205–224.
- Chambers, J.E., Wetherill, G.W., 2001. Planets in the asteroid belt. *Meteorit. Planet. Sci.* 36, 381–399.
- Chambers, J.E., Cassen, P., 2002. Planetary accretion in the inner Solar System: dependence on nebula surface density profile and giant planet eccentricities. *Meteorit. Planet. Sci.* 37, 1523–1540.
- Chambers, J.E., 2003. The formation of life-sustaining planets in extrasolar planetary systems. In: *Proc. Lunar Planet. Sci. Conf. 34th*, League City, TX. Abstract 2000.
- Drake, M.J., Righter, K., 2002. What is the Earth made of? *Nature* 416, 39–44.

- Dreibus, G., Wanke, H., 1989. Supply and loss of volatile constituents during the accretion of terrestrial planets. In: Atreya, S.K., Pollack, J.B., Matthews, M.S. (Eds.), *Origin and Evolution of Planetary and Satellite Atmospheres*. Univ. of Arizona Press, Tucson, pp. 268–288.
- Fegley Jr., B., 2000. Kinetics of gas–grain reactions in the solar nebula. *Space Sci. Rev.* 92, 177–200.
- Goldreich, P., Ward, W.R., 1973. The formation of planetesimals. *Astrophys. J.* 183, 1051–1061.
- Hayashi, C., 1981. Structure of the solar nebula, growth and decay of magnetic fields and effect of magnetic and turbulent viscosities on the nebula. *Prog. Theor. Phys. Suppl.* 70, 35–53.
- Kasting, J.F., 1988. Runaway and moist greenhouse atmospheres and the evolution of Earth and Venus. *Icarus* 74, 472–494.
- Kasting, J.F., Whitmire, D.P., Reynolds, R.T., 1993. Habitable zones around main sequence stars. *Icarus* 101, 108–128.
- Kleine, T., Munker, C., Mezger, K., Palme, H., 2002. Rapid accretion and early core formation on asteroids and the terrestrial planets from Hf–W chronometry. *Nature* 418, 952–955.
- Kokubo, E., Ida, S., 2000. Formation of protoplanets from planetesimals in the solar nebula. *Icarus* 143, 15–27.
- Kokubo, E., Ida, S., 2002. Formation of protoplanet systems and diversity of planetary systems. *Astrophys. J.* 581, 666–680.
- Kominami, J., Ida, S., 2002. The effect of tidal interaction with a gas disk on formation of terrestrial planets. *Icarus* 157, 43–56.
- Leger, A., Selsis, F., Sotin, C., Guillot, T., Despois, D., Mawet, D., Ollivier, M., Labeque, F.A., Valette, C., Brachet, F., Chazelas, B., Lammer, H., 2004. A new family of Planets? “Ocean-planets.” *Icarus*. In press.
- Levison, H.F., Lissauer, J.J., Duncan, M.J., 1998. Modeling the diversity of outer planetary systems. *Astron. J.* 116, 1998–2014.
- Levison, H.F., Agnor, C., 2003. The role of giant planets in terrestrial planet formation. *Astron. J.* 152, 2692–2713.
- Lissauer, J.J., 1993. Planet formation. *Annu. Rev. Astron. Astrophys.* 31, 126–174.
- Lunine, J.I., Chambers, J., Morbidelli, A., Leshin, L.A., 2003. The origin of water on Mars. *Icarus* 165, 1–8.
- Matsui, T., Abe, Y., 1986. Impact-induced atmospheres and oceans on Earth and Venus. *Nature* 322, 526–528.
- Meier, R., Owen, T.C., Jewitt, D.C., Matthews, H.E., Senay, M., Biver, N., Bockelee-Morvan, D., Crovisier, J., Gautier, D., 1998. Deuterium in Comet C/1995 O1 (Hale–Bopp): detection of DCN. *Science* 279, 1707–1710.
- Melosh, H.J., 2003. The history of air. *Nature* 424, 22–23.
- Morbidelli, A., Chambers, J., Lunine, J.I., Petit, J.M., Robert, F., Valsecchi, G.B., Cyr, K.E., 2000. Source regions and timescales for the delivery of water on Earth. *Meteorit. Planet. Sci.* 35, 1309–1320.
- Murray, C.D., Dermott, S.F., 2001. *Solar System Dynamics*. Cambridge Univ. Press, Cambridge, UK.
- Pollack, J.B., Hubickyj, O., Bodenheimer, P., Lissauer, J.J., Podolak, M., Greenzweig, Y., 1996. Formation of the giant planets by concurrent accretion of solids and gas. *Icarus* 124, 62–85.
- Quinn, T.R., Tremaine, S., Duncan, M., 1991. A three million year integration of the Earth’s orbit. *Astron. J.* 101, 2287–2305.
- Robert, F., 2001. The origin of water on Earth. *Science* 293, 1056–1058.
- Sasselov, D.D., Lecar, M., 2000. On the snow line in dusty protoplanetary disks. *Astrophys. J.* 528, 995–998.
- Stevenson, D.J., Lunine, J.I., 1988. Rapid formation of Jupiter by diffusive redistribution of water vapor in the solar nebula. *Icarus* 75, 146–155.
- Yin, Q., Jacobsen, S.B., Yamashita, K., Blichert-Toft, J., Telouk, P., Albarède, F., 2002. A short timescale for terrestrial planet formation from Hf–W chronometry of meteorites. *Nature* 418, 949–952.
- Youdin, A.N., Shu, F.H., 2002. Planetesimal formation by gravitational instability. *Astrophys. J.* 580, 494–505.